Materials Science-Poland, 36(4), 2018, pp. 570-583
http://www.materialsscience.pwr.wroc.pl/
DOI: 10.2478/msp-2018-0090

Nanostructured device based on coated ZnO layer as a window in solar cell applications

H. MOKHTARI[1,2], M. BENHALILIBA[1,2,*], A. BOUKHACHEM[3], M.S. AIDA[4], Y.S. OCAK[5]

[1]Physics Faculty, USTOMB University POBOX 1505 Mnaouer, 31130 Oran, Algeria
[2]Film Device Fabrication-Characterization and Application FDFCA Research Group USTOMB, 31130 Oran, Algeria
[3]Unité de Physique des Dispositifs à Semiconducteurs Université de Tunis El Manar, 2092 Tunis, Tunisia
[4]Laboratory of thin films and plasma Mentouri University, 25000 Constantine, Algeria
[5]Department of Science, Faculty of Education, Dicle University, Diyarbakır, Turkey

This work highlights some physical properties related to the influence of aluminum, tin and copper incorporation on nanostructured zinc oxide (ZnO:M; M:Al, Sn and Cu) thin films prepared by ultrasonic spray pyrolysis technique (USP) on glass substrate at 350±5 °C. For the as-grown layers, M- to Zn-ratio was fixed at 1.5 %. The effects of metal doping on structural, morphological, optical and electrical properties were investigated. X-ray diffraction pattern revealed that the as-prepared thin films crystallized in hexagonal structure with (0 0 2) preferred orientation. The surface topography of the films was performed by atomic force microscopy. AFM images revealed inhibition of grain growth due to the doping elements incorporation into ZnO matrix, which induced the formation of ZnO nanoparticles. Optical measurements showed a high transparency around 90 % in visible range. Some optical parameters, such as optical band gap, Urbach energy, refractive index, extinction coefficient and dielectric constant were studied in terms of doping element. Particularly, dispersion of refractive index was discussed in terms of both Cauchy and single oscillator model proposed by Wemple and DiDomenico. Cauchy parameters and single oscillator energy E_0 as well as dispersion energy E_d were calculated. Finally, electrical properties were investigated by means of electrical conductivity and Hall effect measurements. The measurements confirmed n type conductivity of the prepared thin films and a good agreement between the resistivity values and the oxidation number of doping element. The main aim of this work was the selection of the best candidate for doping ZnO for optoelectronics applications. The comparative study of M doped ZnO (M:Al, Sn and Cu) was performed. High rectifying efficiency of the Al/n-ZnO/p-Si/Al device was achieved and non-ideal behavior was revealed with $n > 4$.

Keywords: *nanostructured ZnO; spray pyrolysis; structural properties; optical properties; electrical measurements; ideality factor*

1. Introduction

Zinc oxide (ZnO) is a II-VI oxide semiconductor with a wide direct band gap energy of 3.3 eV at room temperature; hence, it is highly transparent in the visible region with a sharp cut-off around 380 nm [1, 2]. Due to their physical properties ZnO thin films are widely used in various important applications, such as gas sensors [3–7], light-emitting diodes [8–10], solar cells [11, 12], surface acoustic devices [13–15], transparent electrodes [16], and many others [17–19]. Optical properties of these materials can be easily fine-tuned by controlling the dopant concentration. Though a great deal of excellent work has been reported on such materials [15–17], it is still meaningful to extend the research of these transparent conductive oxide (TCO) thin films.

It has been reported that the band structure and optical properties of ZnO are similar to GaN which is commonly used for the fabrication of photonic devices in the UV range. ZnO has a large excitonic binding energy of 60 meV at room temperature which is larger than that of GaN (25 meV), making it suitable for exciton related applications due to the extreme stability of excitons [20, 21]. ZnO has high mechanical, thermal, and chemical

*E-mail: mbenhaliliba@gmail.com

© 2018. This is an open access article distributed under the Creative Commons Attribution-NonCommercial-NoDerivatives 4.0 License. (http://creativecommons.org/licenses/by-nc-nd/4.0/)

stabilities and radiation hardness [22]. Due to these attractive features, ZnO nanostructures have gained significant attention.

To meet the requirements in different application domains, ZnO is doped with a variety of ions [23–25]. Several techniques, such as metal-organic chemical vapor deposition (MOCVD) [26], chemical vapor transport (CVT) [27], sputtering or spraying [28] and laser ablation [29, 30] have been used to prepare thin films of such type to suit the needs of research and industry. These techniques are generally either sophisticated or expensive, hence, the need for a simple, easy and less expensive technique. In comparison with other techniques, spray pyrolysis method [31–35] is widely used to prepare oxide thin films. It is also characterized by a uniform size distribution and it provides thin films with grain size which is controlled by doping concentration. Furthermore, this technique leads to a large production area and it is suitable to produce crystallized thin films without use of thermal processing [36–40]. In order to provide some interesting properties, several elements, such as indium [31, 41], silver [42], copper [43], tin [44], molybdenum [40], ytterbium [31] and lanthanum [45] may be used as dopants.

In the present paper, we investigate the effect of copper, aluminum and tin incorporation on the structural, electrical and optical properties of ZnO sprayed thin films in order to fabricate optoelectronic devices, gas sensors and photovoltaic systems. To reach our aim, we have fabricated a device based on ZnO layers and contacts thermally evaporated in vacuum. The current-voltage characteristics were plotted and many parameters such as ideality factor, saturation current, series resistance and barrier height using Cheung-Cheung approximation have been extracted.

2. Experimental

2.1. ZnO films and device preparation

ZnO thin films have been first prepared on an ordinary cleaned glass at substrate temperature of 350 °C. 0.1 M of zinc acetate $Zn(CH_3CO_2)_2$ dissolved in a solution containing a mixture of water and propanol in a ratio of 1:1. The precursor mixture was acidified using acetic acid (pH = 5). The mixture was magnetically stirred at 60 °C for 30 min to get a homogeneous structure. The carrier gas – nitrogen was introduced through a 0.5 mm diameter nozzle. The nozzle-to-substrate plane distance was fixed at the optimal value of 20 cm. During the whole deposition process, precursor mixture flow rate was approximately 20 mL/min.

Pure zinc oxide was doped with aluminum, tin and copper to make the solutions of aluminum nitrate $(AlNO_3)_3$, tin chloride $(SnCl_2)$ and copper acetate Cu $(CH_3COO)_2$, respectively. The dopants were added into the solution at a fixed concentration of 1.5 %. The Al/n-ZnO/p-Si/Al device was prepared from 0.1 M of ZnO precursor by spin coating route onto p type silicon and Al contacts were thermally evaporated in vacuum at low pressure of 1.33×10^{-4} Pa using a mask. Al-contacts were circular having a diameter of 1.5 mm. The p-Si wafer with (1 0 0) orientation and resistivity vaying from 1 Ω·cm to 10 Ω·cm was used to produce the contacts. The Al metal thickness was measured as 200 nm. The wafer was degreased for 5 min in boiling trichloroethylene and then rinsed by ultrasonic vibration in acetone and methanol to remove organic contaminations. To remove native oxide layer on the surface, it was etched in HF-H_2O (1:10) solution.

2.2. Characterization techniques

The structural analysis of obtained thin films was performed by means of Bruker D8 ADVANCE with DAVINCI X-ray diffractometer using monochromatic CuKα radiation (λ = 1.54 Å) in the range of 2θ (20° to 80°). The 3D surface topography of as-grown films was performed in taping mode by an atomic force microscopy (NANOSURF). On the other hand, the optical transmittance T (λ) and reflectance R (λ) of ZnO doped films were recorded using a Schimadzu UV 3600 double-beam spectrophotometer in a 300 nm to 2000 nm wavelength domain. Finally, the electrical properties were measured using an ECOPIA

3000 (HMS) Hall effect measurement system at room temperature equipped with S/N magnet with intensity of 0.58 T.

3. Results and discussion

3.1. Structural properties

Fig. 1 shows XRD spectrum of prepared ZnO films. It depicts the presence of (0 0 2), (1 0 2) and (1 1 2) peaks corresponding to hexagonal wurtzite phase according to JCPDS Card No. 05-0664 [46, 47]. The peak detected in pure, Al and Sn doped ZnO layers and located at 52° corresponds to (2 2 0) plane of ZnO_2. Also, in the spectra, a very small amount of (2 0 2) and (1 3 2), corresponding to orthorhombic zinc hydroxide, is observed [48].

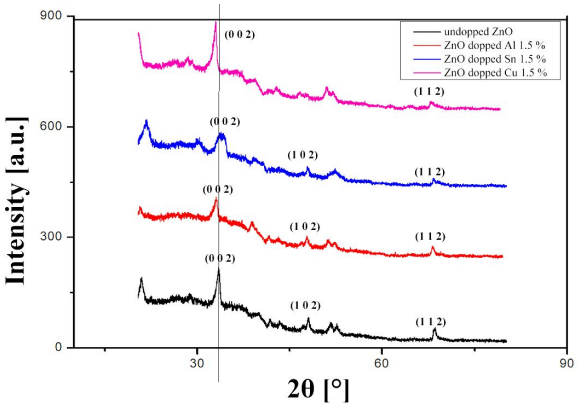

Fig. 1. X-ray diffraction spectra of pure and 1.5 % Al, Sn and Cu doped ZnO sprayed thin films.

The presence of these entities may be explained by the use of methanol and zinc acetate solutions in the ZnO thin films preparation according to the following reaction:

$$2CH_3OH + Zn(CH_3COO)_2 \rightleftarrows Zn(OH)_2 + 2CH_3 - COO - CH_3 + 2H_2O \quad (1)$$

Taking into account that the deposition takes place at a temperature above 200 °C, the zinc hydroxide is transformed into zinc oxide by the following reaction:

$$Zn(OH)_2 \rightleftarrows ZnO + H_2O \quad (2)$$

This transformation is not completed at the preparation temperature of 350 °C and therefore the prepared thin films are characterized by the presence of some entities of $Zn(OH)_2$ type. The presence of these entities plays an important role in the optical and electrical properties of the prepared thin films. Moreover, the interplanar spacing d_{hkl} values were calculated based on the principal phase by using Bragg equation;

$$2d_{hkl}\sin\theta = n\lambda \quad (3)$$

where n is the order of diffraction (usually n = 1) and λ is the X-ray wavelength.

In a hexagonal structure case, it is known that interplanar spacing values d_{hkl} are related to Miller indices (h k l) and the lattice parameters a and c by the following relation [40];

$$\frac{1}{d_{hkl}^2} = \frac{4}{3}\left(\frac{h^2 + hk + k^2}{a^2}\right) + \frac{l^2}{c^2} \quad (4)$$

Using the characteristic relation of the hexagonal structure linking the interplanar spacing with the mesh parameters and the Miller indices, the calculated values of the interplanar spacing were used for the calculation of lattice parameters by the resolution of the following equation system:

$$d_{002(theo)} = d_{002(exp)} \quad (5)$$

$$d_{112(theo)} = d_{112(exp)} \quad (6)$$

where $d_{002(theo)}$ and $d_{002(exp)}$ are respectively theoretical and experimental interplanar spacing of (0 0 2) orientation; and $d_{112(theo)}$ and $d_{112(exp)}$ are respectively the theoretical and experimental interplanar spacing of (1 1 2) orientation. The calculated values of lattice parameters a and c are listed in Table 1.

This result is consistent with the other, indeed, it is found that the two lattice parameters a and c of the deposited films depend on the doping element, which can be considered as a strong argument for the elements penetration into the ZnO matrix. However, the changes in the cell volume as well as the c/a ratio are not in good agreement with the hexagonal mesh and with the ionic radii of Zn^{2+}, Cu^{+}, Al^{3+} and Sn^{4+} ions [50]. This is probably a result of numerous additional mechanisms,

Table 1. Lattice parameters a and c, unit cell volume V, c/a ratio of pure and 1.5 % Al, Sn and Cu doped sprayed ZnO layers.

	a [Å]	c [Å]	V [Å^3]	c/a
ZnO	3.1775	5.3489	46.7708	1.683
ZnO:Cu	3.2008	5.4261	48.1448	1.695
ZnO:Al	3.1906	5.4054	47.6554	1.694
ZnO:Sn	3.2076	5.2846	47.0869	1.648

which occur during the formation of the thin film, leading to the occurrence of defects such as dislocations, interstitial zinc and oxygen deficiency as well as traces of zinc hydroxide. Moreover, regarding the XRD peak intensities, it has been found that the (0 0 2) peak is higher than others. Consequently, (0 0 2) is the preferential orientation of the prepared films. The (0 0 2) peak intensity is different for each dopant. (0 0 2) intensity decreases in Al, and Sn doped ZnO, which may be explained by the fact that aluminum and tin create nucleation sites which, in turn, inhibit the growth of crystal grains. Similar trend was reported by Prajapati et al. [51].

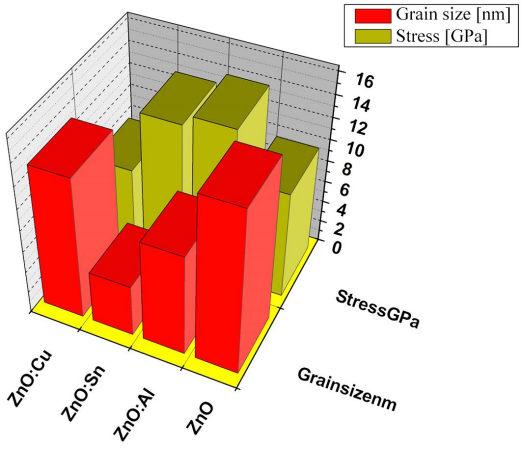

Fig. 2. Grain size and stress in pure and Al, Sn and Cu doped ZnO films.

The intensity of (0 0 2) peak in Cu-doped ZnO is clearly higher than in the pure film. It can be explained by the fact that the film (ZnO:Cu) is thicker than pure ZnO film. It is also shown that there is a slight shift in Bragg angle, depending on the selected dopant. The shift from a bigger angle in Al, and Cu doped ZnO to a smaller angle in Sn-doped ZnO is due to the fact that the substitution of Zn by Al or Cu results from the lattice spacing in Zn (d = 2.65 Å) which is smaller than that of Al, Cu (d = 2.70 Å). The lattice spacing of Sn (d = 2.60 Å) may explain the shift to smaller angles. Sahal et al. [52] reported similar results. Following these observations in terms of (0 0 2) preferential orientation and in view of the existence of the defects, special attention was paid to the dislocations on the basis of the (0 0 2) preferential orientation.

Firstly, the crystallites size was calculated using Debye-Scherer formula [40, 50–53]:

$$D = \frac{k \cdot \lambda}{\beta \cos\theta} \tag{7}$$

k = 0.90 is the Scherrer constant, λ = 1.54 Å is the wavelength of CuKα radiation, β is the (0 0 2) full width at half maximum and 2θ is the Bragg diffraction angle.

Secondly, the interfacial contacts between the crystallites are studied by means of residual stress using the following relation [50–53]:

$$\varepsilon = \frac{\beta}{4\tan\theta} \tag{8}$$

Finally, the dislocation density, which represents the number of dislocation lines per unit area, is estimated by the following equation [50–53]:

$$\delta = \frac{1}{D^2} \tag{9}$$

The calculated values of these structural parameters are listed in Table 2. This structural calculation confirms that this binary oxide exhibits some defects, in particular dislocations and strain, which is consistent with the suggestion mentioned above.

Also, it can be seen that the dislocation density increases with the difference between the ionic radius of Zn^{2+} ion and the ion related to the doping element.

Fig. 2 shows comparative plots between crystallites size and stress and it reveals that the grain

Table 2. Bragg angle, grain size, residual stress, microstrain, dislocation density and crystallinity percent of pure and 1.5 % Al, Sn and Cu doped sprayed ZnO layers.

Samples	$2\theta_{(002)}$ [°]	G [nm]	ϵ	σ [GPa]	δ (10^{14} × lines per m^2]	Crystallinity [%]
Pure ZnO	33.48	15.23	78.99	9.92	43.11	31.1
ZnO:Al	33.07	9.46	128.70	14.19	111.74	17.4
ZnO:Sn	34.00	4.82	245.88	13.24	430.43	45.9
ZnO:Cu	33.07	13.16	92.51	7.68	57.74	24.4

size decreases with increasing stress, which may explain the value of crystallite size by the high amount of stress in our films. These defects seem to be the result related to an additional mechanism caused by the difference between the ionic radius of zinc and doping element, which occurs during the thin film formation. This result is beneficial for possible gas sensor devices and it opens the way to interesting environmental applications [3, 7]. On the other hand, the values of these structural parameters confirm the oxidation number variation. Indeed, the crystallite size decreases with oxidation number contrary to stress and dislocation density, which increase with the oxidation number.

3.2. Atomic force microscopy (AFM) observations

In order to reinforce XRD analysis in terms of incorporation of doping element in ZnO matrix, the surface morphology of sprayed ZnO (pure and MZO with M:Al, Sn and Cu) thin films was investigated using atomic force microscopy. The AFM images show the effect of doping on surface morphology as displayed in Fig. 3.

The observations reveal a decrease in grain size related to incorporation of doping element. This phenomenon is probably related to the decrease of the interstitial zinc which plays an important role in controlling the grains growth of ZnO, due to the introduction of dopant impurities (Al, Sn and Cu) [54]. It may also mean that the grain growth has been inhibited due to the retarding force within the wurtzite structure opposing the driving force of the growth provided by substituted dopant atoms [55].

3.3. Optical properties

3.3.1. Absorption coefficient and Urbach energy

The electronic structure of pure and doped ZnO layers is characterized by the band gap, which defines the energy interval between valence band and conduction band, each of which has a high density of states. This parameter was investigated through the absorption, which was deduced from reflectance and transmittance measurements by UV-Vis spectroscopy. Fig. 4 shows the reflectance and the transmittance spectra of ZnO:M (M = Cu, Al or Sn) sprayed thin films, respectively.

It is noted that the reflectance R is of the order of 20 %, whereas the transmittance T is relatively high in the visible and infrared ranges. This result leads to a low absorption in the visible and near infrared range, which offers the possibility to use these layers as optical windows. The absorption coefficient of as-grown ZnO thin film was determined from transmittance and reflectance measurements using the approximate formula [40]:

$$\alpha = \frac{1}{e}\ln\left(\frac{(1-R)^2}{T}\right) \tag{10}$$

As ZnO is a direct transition semiconductor, the band gap energy Eg was estimated by Tauc law. Indeed, the theory of optical absorption gives the relationship between the absorption coefficient α and the photon energy hν for direct allowed transition as [56]:

$$(\alpha h\nu) = A(h\nu - E_g)^n \tag{11}$$

where α is absorbance coefficient, A is a constant, h is Planck constant, ν is photon frequency, E_g is

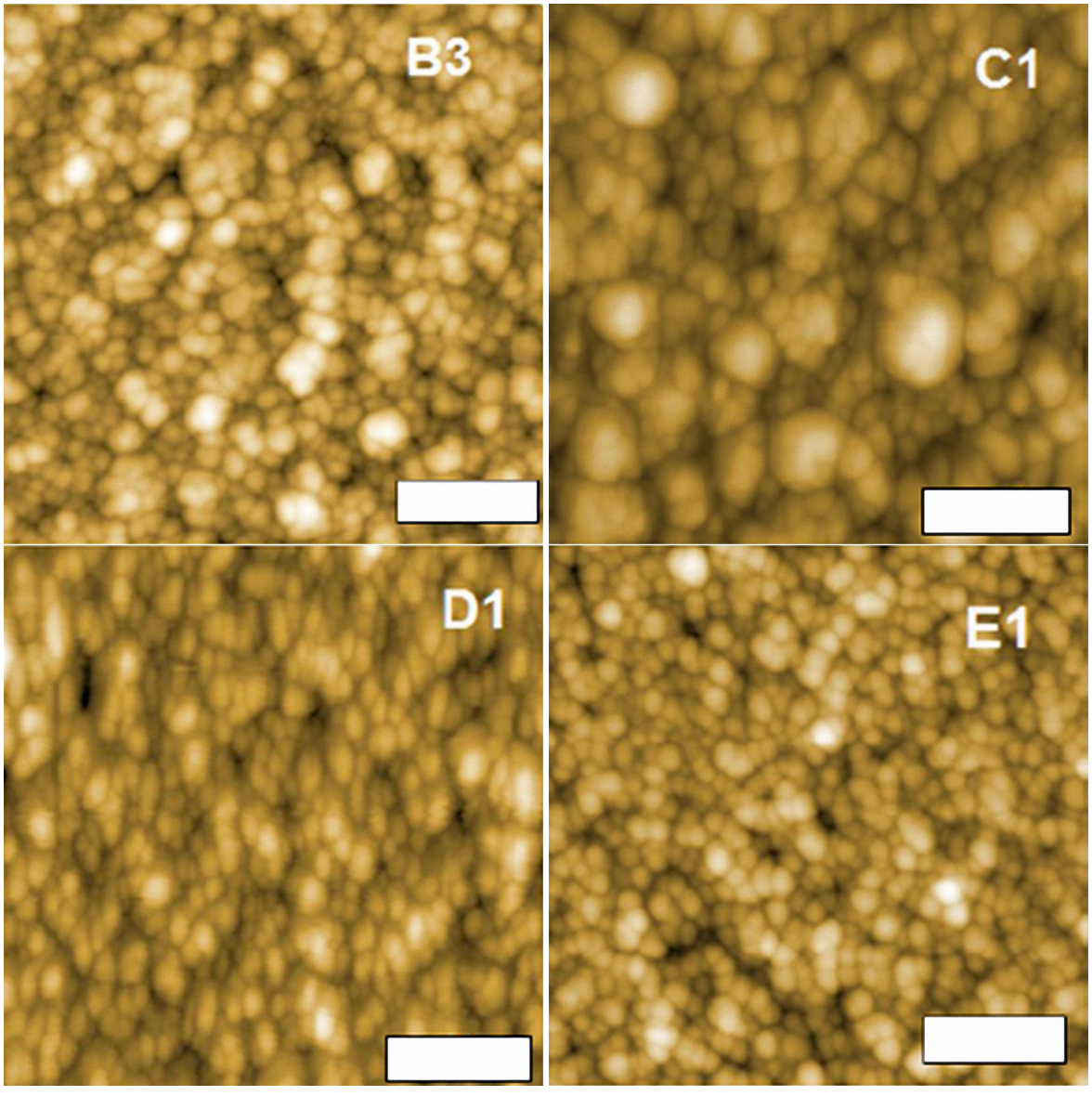

Fig. 3. Surface area (1 μm × 1 μm) scanned by AFM of sprayed ZnO films (from the top to the bottom) 2D view of pure (B3) and Al (C1), Sn (D1) and Cu (E1)-doped ZnO, the white solid bar indicates a scale of 0.25 μm.

optical band gap and n is 1/2 for direct band gap semiconductors. Fig. 5 shows the plot of $(\alpha h\nu)^2$ vs. photon energy which yields the sharp absorption edge for the high quality films by a linear fit. The calculated values of optical band gap E_g of doped ZnO films are summarized in Table 3.

By studying the transmission variation versus photon wavelength, it has been found that the first derivative $dT/d\lambda$, as sketched in Fig. 6, exhibits a peak whose center λ_g can be related to the gap energy $E_g = hc/\lambda_g$. But the width of this peak does not correspond to an ideal material. In effect, for an ideal material, the transmission is zero for the wavelengths lesser than λ_{Eg} (λ_{Eg} is the wavelength calculated at E_g).

In this case, the first derivative presents itself as a Dirac peak. Fig. 7 shows schematically the variation of the transmission and its first derivative as a function of the wavelength normalized with respect to the wavelength of the gap. On the other hand,

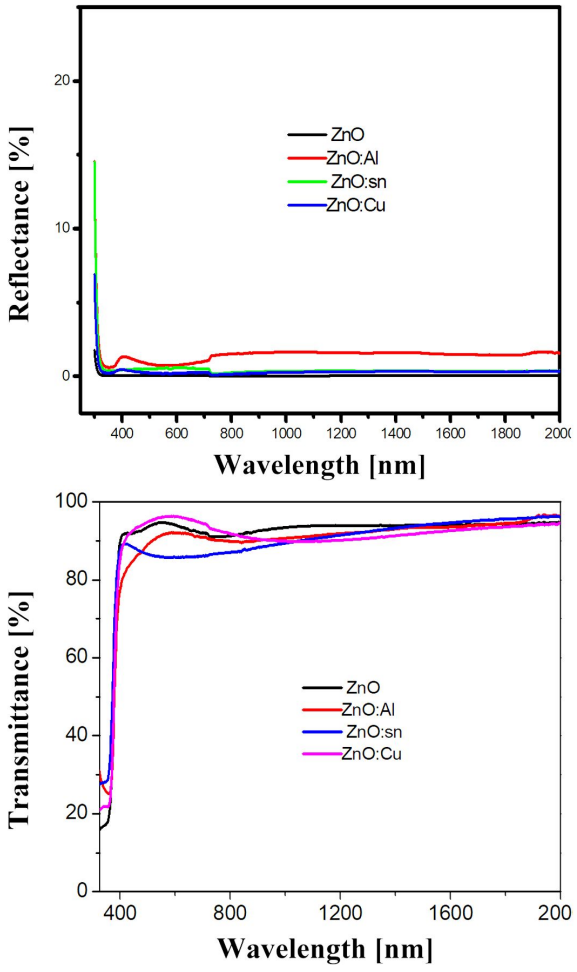

Fig. 4. Reflectance and transmittance spectra of ZnO doped thin films.

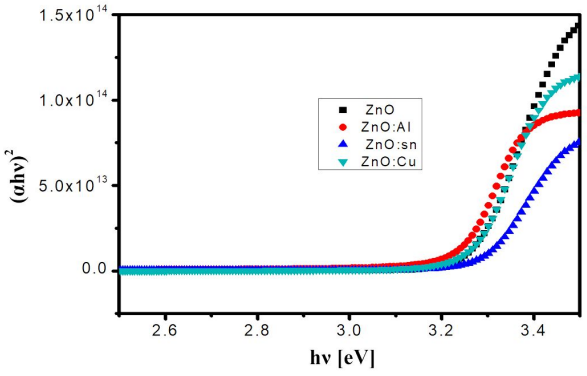

Fig. 5. Plot of $(\alpha h\nu)^2$ vs. photon energy of pure and 1.5 % Al, Sn and Cu doped sprayed ZnO layers.

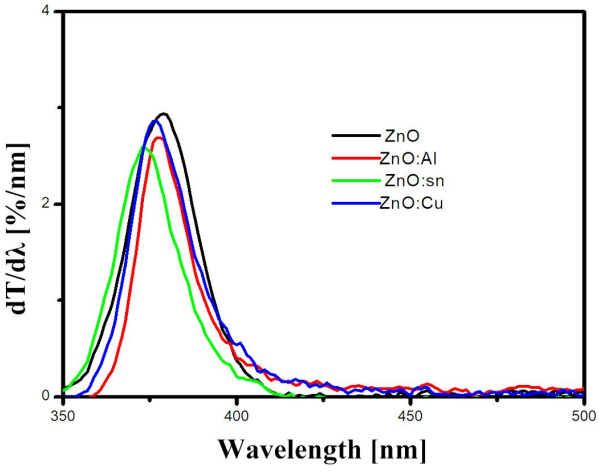

Fig. 6. Variation of dT/dλ vs. wavelength of pure and Al, Sn, Cu doped ZnO layers.

Table 3. Calculated values of optical band gap and Urbach energy of pure and 1.5 % Al, Sn and Cu doped sprayed ZnO layers.

Samples	E_g [eV]	E_U [meV]
ZnO	3.265	91.23
ZnO:Al	3.228	126.63
ZnO:Sn	3.287	111.20
ZnO:Cu	3.260	112.53

it is also found that the thin films absorb even low energy gap energies as seen in Fig. 6.

This phenomenon is due to the presence of localized defect states in the band gap of sprayed ZnO thin film. These localized defect states produce an absorption tail extending deep into the forbidden gap. Indeed, in an ideal material, the band is empty; deformation of equal-energy surface and spreading of these state densities are due to defects [57]. This is consistent with the findings reported by Mott et al. [58] and Kleider et al. [59] indeed, in contrast to the crystalline structures, where the fundamental edge is mainly determined by the conduction band and valence band. This tail is referred as Urbach tail and the associated energy as Urbach energy [60, 61]. According to Urbach law, the absorption coefficient α near the band edge is an exponential function of photon energy as follows [60–62]:

$$\alpha = \alpha_0 \exp\left(\frac{h\nu}{E_U}\right) \tag{12}$$

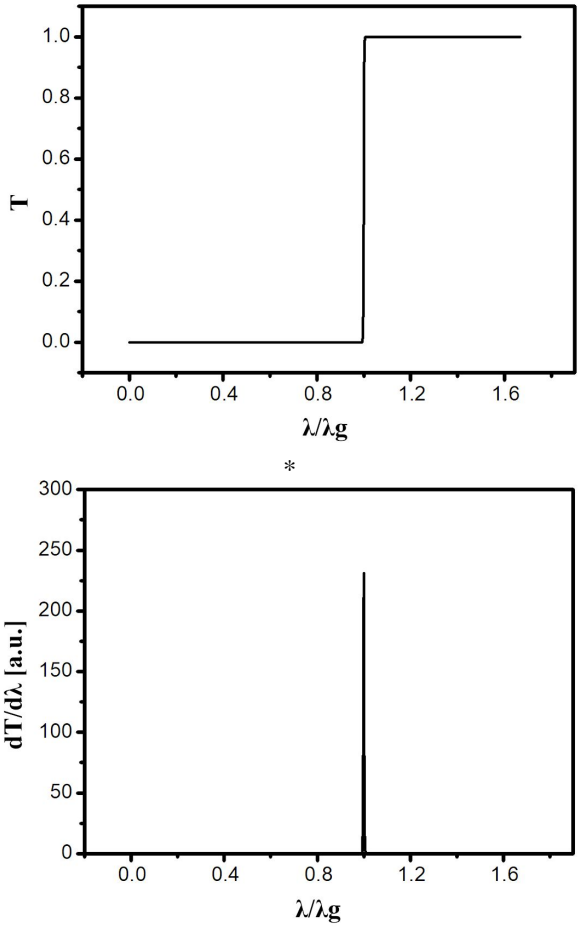

Fig. 7. Schematic variation of the transmittance (a) and its first derivative (dT/dλ) (b) with wavelength.

where α_0 is a constant and E_U is Urbach energy which is interpreted as the width of the tail of the states localized close to the conduction band gap and it determines the width of the band tails of the localized states. Urbach energy value is deduced from the (lnα) against hν curve as shown in Fig. 8. Indeed, the reciprocal of the slope of linear portion below optical band gap, gives the value of E_U:

$$E_U = \left(\frac{d(h\nu)}{d(\ln \alpha)} \right) \tag{13}$$

Fig. 8 shows the logarithm of absorption coefficient α of pure and doped ZnO layers vs. photon energy hν.

It can be seen that Urbach energy depends on doping element. Doping element increases E_U from 91 meV to 126.6 meV for Al doped ZnO layer

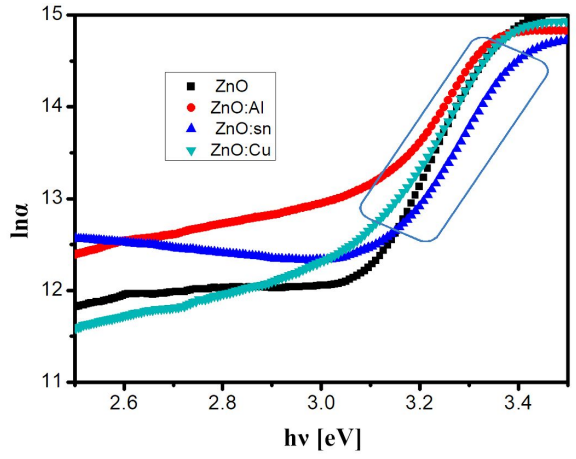

Fig. 8. Plot of lnα versus hν of pure and 1.5 % Al, Sn and Cu doped sprayed ZnO layers.

as listed in Table 3. This result shows the difference in incorporation type of these elements in ZnO matrix. Also, by examining the difference in ionic radii between zinc and the doping elements and the difference in oxidation number (ON), as listed in Table 4, there is a strong correlation with the Urbach energy. It confirms that incorporation of these doping elements into ZnO matrix introduces some defects into the energy bands.

This result reinforces the structural studies described above. The band tails in optical absorption of doped ZnO thin layers may originate from broadening of impurity levels due to their spatial overlap into conduction band and the non-homogenous distribution of impurities.

3.3.2. Opto-thermal investigation

Regarding the value of the band gap energy of the sprayed ZnO thin film which is required to using such films as optical window in solar cells, it is important to study absorptivity of such binary thin films. This issue has been investigated by means of opto-thermal properties.

The effective absorptivity as defined in many precedent studies [63, 64], is the mean normalized absorbance weighed by the $I_{AM1.5}$ solar standard irradiance:

Table 4. Difference of ionic radii and oxidation number in correlation with Urbach energy.

Doping element	$\lvert r^{2+}_{Zn} - r_{doping\ ion}\rvert$ [Å]	$\lvert ON^{2+}_{Zn} - ON_{doping\ ion}\rvert$	E_U [meV]
Al	0.205	1	126.63
Sn	0.05	2	111.20
Cu	0.03	1	112.53

$$\hat{\alpha} = \frac{\int_{\lambda_{min}}^{\lambda_{max}} I_{AM1.5}\alpha(\lambda)d\lambda}{\int_{\lambda_{min}}^{\lambda_{max}} I_{AM1.5}d\lambda} \tag{14}$$

where $I_{AM1.5}$ is the reference solar spectral irradiance, λ is the normalized wavelength and α(λ) is the normalized absorbance spectrum. The absorptivity values are listed in Table 5.

It is known that absorption of a light wave is reflected by a kinetic energy of free charges and therefore the coefficient of absorption increases with the charge density. Moreover, ZnO is a n-type semiconductor, its doping by aluminum which is +3 promotes this type and the doping by tin which is +4 encourages even more the n type of ZnO. But doping by copper ions which are of +1 valence promotes p-type. Indeed, Ahn et al. [65] reported that Cu_2O is a p type semiconductor. This makes that free charge carrier density can be classified as follows:

$$n_{ZnO:Cu} < n_{ZnO} < n_{ZnO:Al} < n_{ZnO:Sn}$$

which is the same as the order of absorptivity.

On the other hand, in comparison with previous work, absorptivity values are less than those of metallic oxide and metallic sulfide such as Al_2O_3 [66], NiO [67], Ag_2S [50], Sb_2S_3 [68] and $LaMnO_{2.75}$ [69]. This shows that ZnO can be considered as one of the best candidates among these materials for such applications as optical window.

3.4. Electrical investigation

Since ZnO is a wide band gap semiconductor, it is interesting to know its electrical properties, particularly the electrical conductivity and the type of charge carriers as well as the influence of doping on these properties. The electrical properties of pure and doped ZnO were investigated by using the conductivity at room temperature and Hall effect measurements. Table 6 summarizes free charge carrier density, mobility, resistivity and Hall coefficient [70, 71].

It was found that doping did not change the n-type of ZnO material. Similarly, absorptivity, and conductivity increased with the oxidation number of the doping element. This is obvious as in the solid state, copper oxide is in Cu_2O form and therefore the oxidation state of the copper is +1. Since zinc has +2 oxidation number, the doping of ZnO by copper favors the p-type and therefore, this doping tends to neutralize the excess of electrons in zinc oxide causing the decreasing of conductivity by copper doping effect. For doping with aluminum which is +3, it is clear that during its incorporation into the ZnO matrix, the aluminum element behaves as a donor which consequently promotes the n type. Finally, for doping with tin element which is +4, the conductivity is greater than that of others. The electric study was followed by further investigation to determine other parameters, such as free charge density n and mobility μ, using the following relations [71]:

$$R_H = \frac{1}{nq} \tag{15}$$

$$\sigma = nq\mu \tag{16}$$

where R_H is Hall coefficient, σ is conductivity and q is electron charge. Free charge carrier density and mobility values are listed in Table 6. It is noted that these two parameters do not obey the same variation pattern with the oxidation number of doping element. For instance, the electrical conductivity is related to several phenomena arising in the doped

Table 5. Absorptivity values of pure and 1.5 % Al, Sn and Cu doped sprayed ZnO thin films.

Sample	ZnO	ZnO:Al	ZnO:Sn	ZnO:Cu
$\hat{\alpha}$ [$\times 10^4$ m^{-1}]	29.91	31.47	34.23	29.44

Table 6. Free charge carrier density, mobility, resistivity, Hall coefficient and conductivity type of pure and 1.5 % Al, Sn and Cu doped sprayed ZnO thin films.

Films	n [$10^{12} \times$ cm^{-3}]	μ [cm^2/V·s]	ρ [$10^2 \times \Omega$·cm]	R_H [$10^5 \times$ cm^3/C]	Type
ZnO	1.065	189	309.6	–58.64	n
ZnO:Al	48.23	227	57.01	–12.94	n
ZnO:Sn	50.92	128	9.546	–1.226	n
ZnO:Cu	14.5	39.61	108.7	–4.304	n

materials, such as structural defects, impurities and effect of doping on the effective mass and the collision time.

3.5. I-V characteristics of Al/n-ZnO/p-Si/Al device

The I-V characteristics of the Al/n-ZnO/p-Si/Al device are described by thermionic emission model as follows [72, 73]:

$$I = I_0 \exp\left[\frac{q(V - IR_s)}{nkT}\right] \tag{17}$$

Derivative of voltage over derivative of lnI yields the ideality factor n of device (n = 1 for ideal diode case) as follows [72]:

$$n = \frac{q}{kT}\frac{dV}{d(\ln I)} \tag{18}$$

where I and V are the measured current and applied bias voltage, I_0 is the saturation current expressed as [72]:

$$I_0 = AA^*T^2 \exp\left(-\frac{q\Phi_b}{kT}\right) \tag{19}$$

where A^* is Richardson constant (32 A/K^2·cm^2 for p-type Si) [72], A is effective device area T is the ambient temperature in Kelvin, q is electron charge, Φ_b is zero-bias barrier height of our device expressed as follows [73]:

$$\Phi_b = \frac{kT}{q}\ln\left(\frac{AA^*T^2}{I_0}\right) \tag{20}$$

The as-fabricated device shows a high rectification ratio RR, I (5 V)/I (–5 V), of 44554 as displayed in Fig. 9.

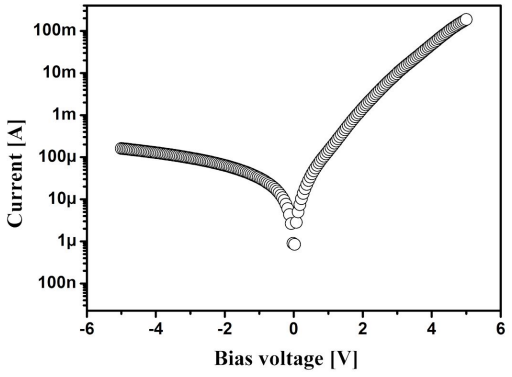

Fig. 9. Room temperature I-V characteristics of Al/n-ZnO/p-Si/Al device in dark within –5 V and +5 V bias voltage range.

The non-ideal behavior of the device was revealed and ideality factor was found to be 4.4. The latter was determined in the forward voltage range according to V > 3 kT/q condition and saturation current I_0 was evaluated as 41.4 nA as shown in Fig. 10.

In order to demonstrate the role of series resistance, Cheung et al. [74] have developed an approximation, in terms of current and voltage, expressed as:

$$\frac{dV}{d(\ln I)} = IR_S + n\left(\frac{kT}{q}\right) \tag{21}$$

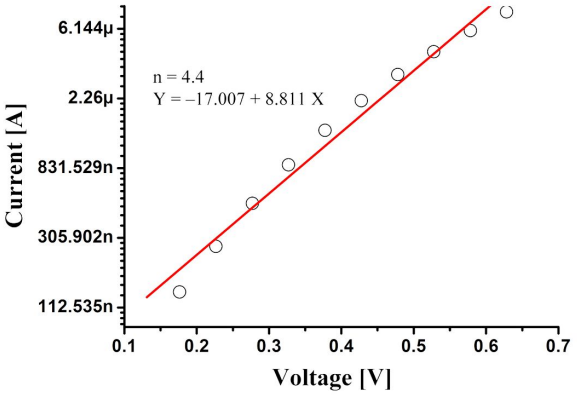

Fig. 10. I-V plots in the forward voltage range of Al/n-ZnO/p-Si/Al device. The linear fit is displayed in red solid straight line; fit equation is displayed inside the figure.

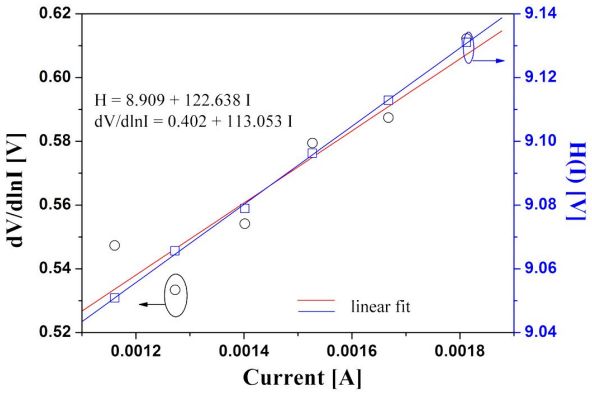

Fig. 11. Double Y-axis plot of variation of dV/dlnI (left) and H (right) versus current for Al/n-ZnO/p-Si/Al device. Straight lines obtained by linear fitting are displayed and fit equations are written inside the figure.

and the function H versus current is written as follows [74]:

$$H(I) = V - \left(\frac{nkT}{q}\right) \ln\left(\frac{I}{AA^{*}T^{2}}\right) \tag{22}$$

Furthermore, it is rewritten in terms of Rs and Φ_b in the following equation [73, 74]:

$$H(I) = IR_S + n\phi_b \tag{23}$$

where A is the contact area evaluated at 0.018 cm^2. Ideality factor and series resistance as well as the barrier height were calculated using Cheung approximation. The parameters extracted from Cheng-Cheung functions were assessed in forward bias voltage and in high current range of 1.2 mA to 1.8 mA as seen in Fig. 11.

Therefore, the profile of quantities dV/dlnI and H(I) vs. I plots for Al/ZnO/Si/Al device under dark and room temperature conditions show roughly a linear increase as displayed in Fig. 11. Series resistance, obtained by (dV/dlnI) vs. I and H vs. I, is around 123 Ω and 113 Ω, respectively. Ideality factor is roughly around 15 and the barrier height is of 0.59 eV as determined by equation 23. This high value of n is due to presence of interface layers and series resistance in our device. The obtained Rs value, determined by Cheung method, ranges within 508 Ω to 534 Ω for Ag/SnO_2:In/Si/Au Schottky diode, while the barrier height is around 0.57 eV as reported previously [75]. Other results, like ideality factor 2.7 to 3.5 for the Ag/SnO_2:In/Si/Au MOS diode when In doping level varied from 4 % to 8 % and Rs ranging from 344 Ω to 538 Ω, obtained using Cheung approximation, have been demonstrated [76]. An organic layer inserted in the junction as Au/PVP/ZnO/Si/Al has changed the value of ideality factor and Rs, which were found to be 4.45 and 30 kΩ, respectively, as previously reported [77].

4. Conclusions

Pure and aluminum, tin and copper doped zinc oxide thin films have been successfully deposited on a glass substrate by spray pyrolysis technique at 350 °C. X-ray diffraction analysis shows that the prepared film are mainly composed of hexagonal wurtzite ZnO phase.

Also the doped thin films show c-axis oriented (0 0 2) plane. The structural parameters (lattice parameters, grain sizes) depend on the doping element. The optical properties deduced from the transmission and reflection spectra show a good transparency of the deposited thin films in the visible and near infrared regions. Optical band gap energy and Urbach energy have been calculated in terms of doping element. The observations

by atomic force microscope show a smooth enough surface which has the potential for optoelectronic applications by minimizing the diffusion caused by irregular surfaces. Besides, the electrical properties of M-doped ZnO thin films have been studied. Moreover, the Hall effect measurements at room temperature give a negative Hall coefficient value which indicates an electronic conduction in the as-grown ZnO thin films.

The electrical conductivity measurements show good agreement with the nature of the doping element and the effect of the oxidation number of doping element on the electrical conductivity as well as on absorptivity. According to this investigation, ZnO is a multifunctional material. In order to show the importance of ZnO for electronic device fabrication, Al/ZnO/pSi/Al device was fabricated and its current-voltage characteristics were measured. High rectifying efficiency of the device was achieved and its non-ideal behavior was revealed ($n > 4$). The device had a relatively high series resistance which was around 123 Ω and barrier height of 0.59 eV. This result is very interesting as by using a simple spray pyrolysis, which is a low-cost technique, it was possible to prepare doped oxides and open the way for possible use of the prepared films in many optoelectronic applications. Further studies on possible environmental applications of the doped films, particularly in gas sensors, photocatalysis and micro-optoelectronic applications, are in progress. ZnO:Al may also be used as a window in solar cells.

Acknowledgements

The work is included in the PNR projects under the Contract No. 8/U311/R77 and U311/R81, supported by the "Agence thematique de recherche en science et technologie" (ATRST) (`http://www.atrst.dz`), and the National Administration of Scientific Research (`http://www.dgrsdt.dz`). This work is a part of the PRFU 2018 Project No. B00L02UN310220180011 supported by the Oran University of Sciences and Technology (`http://www.mesrs.dz`, and `http://www.univusto.dz`). It is included in the ANVREDET Project No. 18/DG/2016 (`http://www.anvredet.dz`).

References

[1] KLINGSHIRN C., *Phys. Status Solidi B*, 71 (1975), 547.
[2] PARK S.-M., IKEGAMI T., EBIHARA K., SHIN P.-K., *Appl. Surf. Sci.*, 253 (2006), 1522.
[3] LOKHANDEA C.D., GONDKARA P.M., RAJARAM S., MANE B., SHINDEA V.R., HANB S.-H., *J. Alloy. Compd.*, 475 (2009), 304.
[4] CHANG J.F., KUO H.H., LEU I.C., HON M.H., *Sensor. Actuat. B-Chem.*, 84 (2002), 258.
[5] ZUNXIAN YANG A., YUN HUANG B., GUONAN CHEN A., ZAIPING GUO C., SHUYING CHENG B., SHIZHEN HUANG E., *Sensor. Actuat. B-Chem.*, 140 (2009), 549.
[6] GRUBER D., KRAUS F., MÜLLER J., *Sensor. Actuat. B-Chem.*, 92 (2003), 81.
[7] PENGA X.Y., SAJJADA M., CHUA J., YANGB B.Q., FENGA P.X., *Appl. Surf. Sci.*, 257 (2011), 4795.
[8] LING B., SUN X.W., ZHAO J.L., TAN S.T., DONG Z.L., YANG Y., YU H.Y., QI K.C., *Physica E*, 41 (2009), 635.
[9] SUN J., FENG Q., BIAN J., YU D., LIA M., LI H., LIANG H., ZHAO J., QIU H., DU G., *J. Lumin.*, 131 (2011), 825.
[10] HWANG S.-H., CHUNG T.-H., LEE B.-T., *Mater. Sci. Eng. B-Adv.*, 157 (2009), 32.
[11] WANG F.-H., CHANG H.-P., TSENG C.-C., HUANG C.-C., LIU H.-W., *Curr. Appl. Phys.*, 11 (2011), 12.
[12] TOMAR M.S., GARIA F.J., *Thin solid Films*, 90 (1982), 419.
[13] KRISHNAMOORTHY S., AGIS A., ILIADI S., *Solid State Electron.*, 52 (2008), 1710.
[14] SHIH W.-C., WANG M.-J., NAN L.I., *Diam. Relat. Mater.*, 17 (2008), 390.
[15] FU Y.Q., LUO J.K., DU X.Y., FLEWITT A.J., LI Y., MARKX G.H., WALTON A.J., MILNE W.I., *Sensor. Actuat. B-Chem.*, 143 (2010), 606.
[16] BENHALILIBA M., BENOUIS C.E., SILVER T.A., *J. Technol. Mater.*, 1 (2011), 24.
[17] OKUR S., YAKUPHANOGLU F., STATHATOS E., *Microelectron. Eng.*, 87 (2010), 635.
[18] DICKHERBER A., CORSO C.D., HUNT D., *Sensor. Actuat. A-Phys.*, 144 (2008), 7.
[19] REYNOLDS D.C., LOOK D.C., JOGAI B., *Solid State Commun.*, 99 (1996), 873.
[20] SHAN F.K., LIU G.X., LEE W.J., SHIN B.C., *J. Appl. Phys.*, 101 (2007), 2437122.
[21] OHSHIMA T., THAREJA R.K., IKEGAMI T., EBIHARA K., *Surf. Coat. Tech.*, 169 (2003), 517.
[22] LUPAN O., PAUPORTE T., CHOW L., VIANA B., PELLE F., ONO L.K., *Appl. Surf. Sci.*, 256 (2010), 1895.
[23] ZHONG W.W., LIU F.M., CAI L.G., ZHOU C.C., DING P., ZHANG H., *J. Alloy. Compd.*, 499 (2010), 265.
[24] SANG B., NAGOYA Y., KUSHIYA K., YAMASE O., *Sol. Energ. Mat. Sol. C.*, 75 (2003), 179.
[25] FU Q., HU L., YU D., SUN J., ZHANG H., HUO B., ZHAO Z., *Mater. Lett.*, 63 (2009), 316.
[26] SHIMOMURA T., KIM D., NAKAYAMA M., *J. Lumin.*, 112 (2005), 191.
[27] HENLEY S.J., ASHFOLD M.N.R., CHERNS D., *Surf. Coat. Tech.*, 177 (2004), 271.
[28] DINESCU M., VERARDI P., *Appl. Surf. Sci.*, 106 (1996), 149.

[29] CHENG B.C., XIAO Y.H., WU G.S., ZHANG L.D., *Appl. Phys. Lett.*, 84 (2004), 416.
[30] LUCIO-LOPEZ M.A., LUNA-ARIAS M.A., MALDONADO A., LA DE M., OLVERA L., ACOSTA D.R., *Sol. Energ. Mat. Sol. C.*, 90 (2006), 733.
[31] BOUKHACHEM A., FRIDJINE S., AMLOUK A., BOUBAKER K., BOUHAFS M., AMLOUK M., *J. Alloy. Compd.*, 501 (2010), 339.
[32] CHAKRABORTY A., MONDAL T., BERA S.K., SENC S.K., GHOSH R., PAUL G.K., *Mater. Chem. Phys.*, 112 (2008), 162.
[33] HEERDEN VAN J.L., SWANEPOEL R., *Thin Solid Films*, 299 (1997), 72.
[34] BOUBAKER K., CHAOUACHI A., AMLOUK M., BOUZOUITA H., *Eur. Phys. J.-Appl. Phys.*, 37 (2007), 105.
[35] BELGACEM S., BENNACEUR R., *Rev. Phys. Appl.*, 25 (1990), 1245.
[36] LI X.Y., LI H.J., WANG Z.J., XIA H., XIONG Z.Y, WANG J.X., YANG B.C., *Opt. Commun.*, 282 (2009), 247.
[37] PANKOVE J.I., *Optical Processes in Semiconductors*, Prentice-Hall Inc., Englewood Cliffs, NJ, 1971.
[38] ILICAN S., CAGLAR Y., CAGLAR M., *J. Optoelectron. Adv. M.*, 10 (2008), 2578.
[39] PEJOVA B., *Mater. Chem. Phys.*, 119 (2010), 367.
[40] BOUKHACHEM A., OUNI B., KARYAOUI M., MADANI A., CHTOUROU R., AMLOUK M., *Mat. Sci. Semicon. Proc.*, 15 (2012), 282.
[41] BENHALILIBA M., BENOUIS C.E., AIDA M.S., YAKUPHANOGLU F., SANCHEZ JUAREZ A., *J. Sol-gel Sci. Techn.*, 55 (2010), 335.
[42] JAYABHARATHI J., PRABHAKARAN A., THANIKACHALAM V., UNDHARESAN M., *J. Photoch. Photobio. A*, 325 (2016), 88.
[43] SREEDHAR A., KWON J.H., YI J., SU K.J., GWAG J.S., *Mat. Sci. Semicon. Proc.*, 49 (2016), 8.
[44] ISMAIL A.S., MAMAT M.H., SIN N.D., MALEK M.F., ZOOLFAKAR A.S., SURIANI A.B., MOHAMED A., AHMAD M.K., RUSOP M., *Ceram. Int.*, 42 (2016), 9785.
[45] MRABET C., KAMOUN O., BOUKHACHEM A., AMLOUK M., MANOUBI T., *J. Alloy. Compd.*, 648 (2015), 826.
[46] PRAJAPATI C.S., KUSHWAHA A., SAHAY P.P., *Mater. Chem. Phys.*, 142 (2013), 276.
[47] PARAGUAY D.F., MORALES J., ESTRADA L.W., ANDRADE E., MIKI-YOSHIDA M., *Thin Solid Films*, 350 (1999), 192.
[48] COREY R.B., WYCKOFF R.W.G., *ZEKGAX*, 86 (1933), 8.
[49] SHANNON R.D., *Acta Crystallogr. Section A*, 32 (1976), 751.
[50] BOUGHALMI R., BOUKHACHEM A., GAIED I., BOUBAKER K., BOUHAFS M., AMLOUK M., *Mat. Sci. Semicon. Proc.*, 16 (2013), 1584.
[51] PRAJAPATI C.S., KUSHWAHA A., SAHAY P.P., *Mater. Chem. Phys.*, 142 (2013), 123.
[52] SAHAL M., HARTITI B., RIDAH A., MOLLAR M., MARI B., *Microelectron. J.*, 39 (2008), 1425.
[53] EL-NAHASS M.M., FARAG M.A.A., IBRAHIM E.M., ABD-EL-RAHMAN S., *Vacuum*, 72 (2004), 453.
[54] FUJIHARA S., SASAKI C., KIMURA T., *J. Eur. Ceram. Soc.*, 21 (2001), 2109.
[55] KELSALL R.W., HAMLEY I.W., GEOGHEGAN M., *Nanoscale Science and Technology*, John Wiley & Sons, West Sussex, 2005, p. 261.
[56] BENHALILIBA M., BENOUIS C.E., MOUFFAK Z., OCAK Y.S., TIBURCIO-SILVER A., AIDA M.S., GARCIA A.A., TAVIRA A., SANCHEZ JUAREZ A., *Superlattices and Microstructures* 63 (2013), 228.
[57] LOUKIL A., BOUKHACHEM A., AMOR B.M., GHAMNIA M., RAOUADI K., *Ceram. Int.*, 42 (2016), 8274.
[58] MOTT N.F., DAVIS E.A., *Electronic Processes in Non-Crystalline Materials*, Clarendon Press, Oxford, 1979.
[59] KLEIDER J.P., GAUTHIER M., LONGEAUD C., ROY D., SAADANE O., BRÜGGEMANN R., *Thin Solid Films*, 188 (2002), 403.
[60] URBACH F., *Phys. Rev. A*, 92 (1953), 1324.
[61] MARTIENSSEN W., *J. Phys. Chem. Solids*, 21 (1957), 257.
[62] BENOUIS C.E., BENHALILIBA M., SANCHEZ JUAREZ A., AIDA M.S., CHAMI F., YAKUPHANOGLU F., *Journal of Alloys and Compounds*, 490 (2010), 62.
[63] AMLOUK A., BOUBAKER K., AMLOUK M., BOUHAFS M., *J. Alloy. Compd.*, 485 (2009), 887.
[64] BENHALILIBA M., BENOUIS C.E., BOUBAKER K., AMLOUK M., AMLOUK A., *A New Guide to Thermally Optimized Doped Oxides Monolayer Spray-Grown Solar Cells: The Amlouk-Boubaker Optothermal Expansivity ψAB, Solar Cells - New Aspects and Solutions*, InTech Edition, 2011.
[65] AHN J.S., PODE R., LEE K.B., *Thin Solid Films*, 623 (2017), 121.
[66] ARIFA H., BOUKHACHEM A., ASKRI B., BOUBAKER K., YUMAK A., RAOUADI K., *Ceram. Int.*, 42 (2016), 2147.
[67] MRABET C., AMOR B.M., BOUKHACHEM A., AMLOUK M., MANOUBI T., *Ceram. Int.*, 42 (2016), 5963.
[68] BOUGHALMI R., BOUKHACHEM A., KAHLAOUI M., MAGHRAOUI H., AMLOUK M., *Mat. Sci. Semicon. Proc.*, 26 (2014), 593.
[69] BOUKHACHEM A., ZIOUCHE A., AMOR B.M., KAMOUN O., ZERGOUG M., MAGHRAOUI-MEHERZI H., YUMAK A., BOUBAKER K., AMLOUK M., *Mater. Res. Bull.*, 74 (2016), 202.
[70] MOKHTARI H., BENHALILIBA M., AIDA M.S., ATTAF N., OCAK Y.S., *EPJ Web of Conferences*, 44 (2013), 03006.
[71] BENOUIS C.E., BENHALILIBA M., MOUFFAK Z., AVILA-GARCIA A., TIBURCIO-SILVER A., ORTEGA LOPEZ M., ROMANO TRUJILLO R., OCAK Y.S., *Journal of Alloys and Compounds*, 603 (2014), 213.
[72] MISSOUM I., BENHALILIBA M., CHAKER A., OCAK Y.S., BENOUIS C.E., *Synthetic Metals*, 207 (2015), 42.

[73] MISSOUM I., OCAK Y.S., BENHALILIBA M., BENOUIS C.E., CHAKER A., *Synthetic Metals*, 214 (2016), 76.

[74] CHEUNG S.K., CHEUNG N.W., *Appl. Phys. Lett.*, 49 (1986), 85.

[75] BENHALILIBA M., *Journal of Nano- and Electronic Physics*, 7, (2015), 02029.

[76] BENHALILIBA M., BENOUIS C.E., AIDA M.S., AYESHAMARIAM A., *Journal of Semiconductors*, 38 (2017), 064004-1.

[77] MOKHTARI H., BENHALILIBA M., *Journal of Semiconductors*, 38 (2017), 116001-1.

Received 2017-02-14
Accepted 2018-07-11